

# Fundamental and Beam Propagation Behaviour of a Microjet and Recent Applications using Laser MicroJet<sup>®</sup> Technology

T. A. Mai, B. Richerzhagen, K. Stay

Synova SA, Ch. de la Dent-d'Oche 1, CH-1024 Ecublens, Switzerland  
 Phone +41 21 694 35 00; fax +41 21 694 35 01  
 E-mail: mai@synova.ch

The innovative water jet-guided laser technology (also called as Laser MicroJet<sup>®</sup> LMJ) is relatively new. However, due to a number of unique advantages, it has quickly and successfully matured into many applications such as dicing and slotting of silicon wafers, cutting of coronary stents, drilling of stencil and OLED masks, as well as the cutting of hard materials for tool inserts. This cold, clean machining technology allows the precision fabrication of intricate structures, providing exceptional aspect ratios. In this paper, the fundamental behaviour of a hair-thin water jet such as jet velocity, jet break-up and interruptions are studied. A well-rounded understanding of the jet stability characteristics is very important to enhance the performance of the LMJ technology. The propagation and the intensity distribution of a laser beam coupled in the low pressure, laminar water jet at various coupling conditions are theoretically and experimentally investigated as well. The final part of this paper will highlight some recent micromachining examples of the LMJ technology.

**Keywords:** Water guided laser, laser micromachining, cutting, drilling, structuring, jet stability

## 1. Introduction

The relatively new and innovative principle of a water jet-guided laser for micromachining has in a very short time period, made a big impact on the industry [1]. The concept, which functions by funnelling a laser beam through a hair fine jet of low-pressure water, relies on the total internal reflection of the laser beam by the walls of the water jet.

As the diameter of the jet is relatively large with respect to the wavelength of the lasers ( $\approx 1 \mu\text{m}$ ), the water jet can be considered to be a multimode fibre. Propagation of light in multimode fibres is usually characterized by a finite number of guided modes, refractive and tunnelling leaky modes that are partially guided, and a continuum of radiation modes [2]. Many theoretical aspects of propagation of waves in cylindrical waveguides as well as intermodal coupling are discussed in literature [3]. The interference of the modes leads to the modal noise at the exit of the waveguide. Modal noise in optical fibres has been studied starting from the early 80's [4] up to recent reports [5]. For the water jet waveguide, the number of optical modes is high. For big jets, the water jet waveguide is comparable to a large core fibre [6]. The stability of the water jet, characterized by the break-up length, is limited by increasing water surface waves. They are due to initial perturbations [7] and also due to the laser induced break-up [8]. In addition, due to the long interaction length between the high intensity beam of a 100W frequency doubled Nd:YAG laser and water, high efficiency stimulated Raman scattering has been seen in micrometer-sized water jets [9]. In this article, the propagation of a low power and coherent laser light in the water jet waveguide is investigated.

## 2. Laser MicroJet<sup>®</sup> - Principal and Visualisation

### 2.1 Generation of the water jet

The jet is produced by forcing the water, under low pressure, through a sharp edged nozzle in a coupling unit (see Fig. 1).

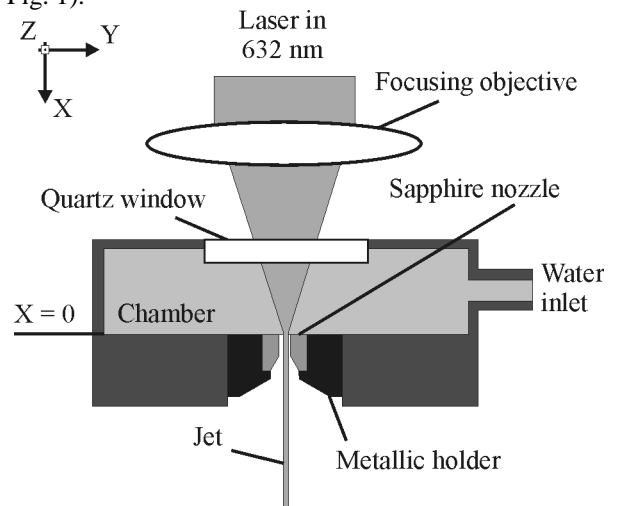


**Fig. 1** Schematic of the coupling unit

The nozzle orifice is made of sapphire or diamond. The resulting diameter of the water jet is about 5% smaller than the nozzle diameter due to the vena contracta effect [10]. The coupling unit consists of a quartz window, a chamber and a nozzle holder where nozzles of different orifice diameters (presently 20-100 $\mu\text{m}$ ) can be installed.

### 2.2 Light coupling into the water jet waveguide

The overall experimental configuration is depicted in Fig. 2., and the water coupling is shown in zone A.

A He-Ne laser ( $\lambda = 632 \text{ nm}$ , 5 mW) was specified as the light source.

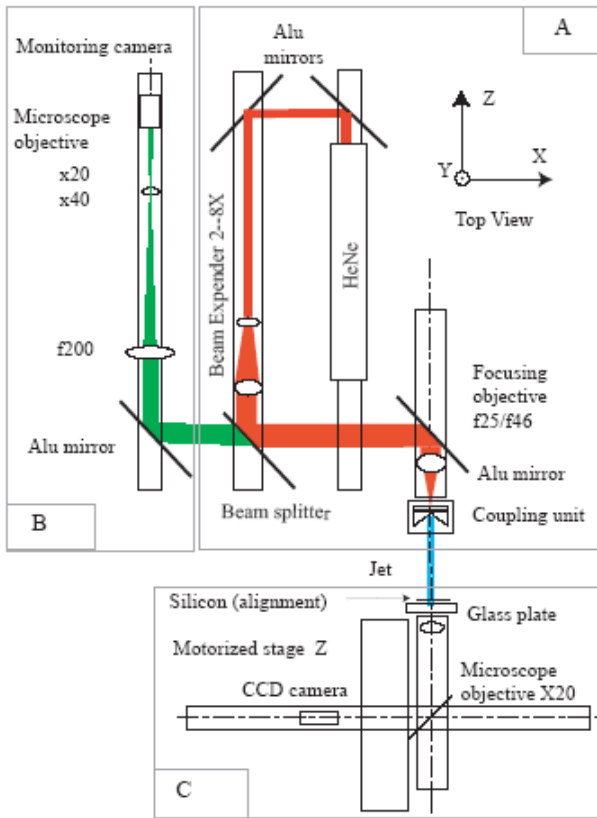


**Fig. 2** Schematic experimental set-up of the He-Ne laser coupling system into waterjet (A), coupling control system (B), waveguide observation system (C)

The coupling into the jet is achieved by increasing the 1 mm diameter beam ( $1/e^2$ ) to a maximum 8 mm  $1/e^2$  with a variable beam-expander (BE) and then focusing with an objective (between  $f = 25 \text{ mm}$  and  $46 \text{ mm}$ ). The water jet interface was calculated using computational fluid dynamic software called “Fluent”. It was immediately visible from this, that the light is guided by the water-air interface.

By varying the ratio of beam expansion and the choice of objective, three values of Numerical Apertures (NA) were tested: 0.06, 0.16 and 0.29. These values correspond to the depth of focus and beam diameters listed in Table 1. The focused laser spot diameter ( $1/e^2$ ) was measured in water at the upper nozzle level. It should be noted that despite these high values of NA, they are still smaller by a factor of more than three times that of the NA of the water jet waveguide ( $NA=0.87$ ).

**Table 1** Depth of focus  $2 \times$ Rayleigh range ( $L_{Ra}$ ) and the focal diameters

Focusing lens	BE	NA	$2L_{Ra}$	$2\omega \cdot \left(\frac{1}{e^2}\right)$
46 mm	No BE	0.06	260 $\mu\text{m}$	15.5 $\mu\text{m}$
46 mm	X8	0.16	42 $\mu\text{m}$	6.8 $\mu\text{m}$
25 mm	X8	0.29	8.6 $\mu\text{m}$	2.6 $\mu\text{m}$

## 2.3 Observation of the modes in the water jet

As shown in zone C of Fig. 2, the glass plate is placed in the path of the jet to visualise the light intensity distribution. High-magnification images were then obtained with the help of a microscope objective ( $\times 10$   $\times 20$ ) located right behind the glass plate and a CCD video camera. The whole imaging system is mounted on a motorized Z stage so that the distance of the glass plate can be varied from the jet origin. The modal noise is then characterized by the modulation wavelength  $\lambda_N$ . It is obtained by image processing using the vertical or horizontal intensity profiles of the jet section.  $\lambda_N$  is then derived from the inverse maximum frequency in the Fourier spectra of the profiles.

## 3. Results of modal noise measurements

### 3.1 Spatial distribution

The increase in the number of modes i.e. the reduction of the size of the speckle grains with increasing NA is demonstrated in Fig. 3, for a nozzle of 112  $\mu\text{m}$  in diameter. In this example the spot is centred with respect to the jet axis. The size of the speckle grains expressed as the characteristic modulation wavelength  $\lambda_N$  are 6  $\mu\text{m}$  and 2.2  $\mu\text{m}$  for  $NA = 0.06$  and 0.29 respectively.

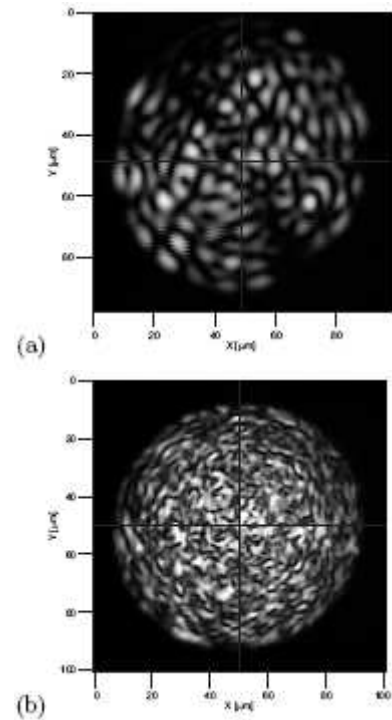


**Fig. 3** Light intensity distribution in the water jet, observed through a glass plate (nozzle diameter 112  $\mu\text{m}$ , centred coupling, jet distance 35 mm, jet velocity 132 m/s). (a)  $NA=0.06$ ; (b)  $NA=0.29$ ; modulation wavelengths: 6 and 2.2  $\mu\text{m}$ .

### 3.2 Mode distribution at different jet diameters

Mode distributions corresponding to nozzles with diameters of 60 and 29  $\mu\text{m}$  are shown in Fig. 4. In this example with  $NA=0.16$ , the laser focus is centred and located at the nozzle entry. Comparing the intensity distributions of

the 122  $\mu\text{m}$  diameter nozzle (Figure 3(b)) with the diameters of 65  $\mu\text{m}$  (Figure 4a) and 29  $\mu\text{m}$  (Figure 4b), a much stronger variation is observed. The images were taken with different values of magnification, as with the decreasing diameter of the water jet, the relative size of the “speckle grains” increases. At 29  $\mu\text{m}$  the presence of few big spots indicates that few modes are guided (see Figure 4b).

For large waveguide diameters, the combination of many modes, results in modal noise where many speckle grains of small size are present. On the contrary, for smaller waveguide diameters, fewer modes are guided and therefore fewer speckle grains, but with a larger size are observed.

### 3.3 Intensity modulation at different coupling NA

In order to understand the observed grain sizes in the intensity distribution, we refer to well-known formulas for fibre optics [11]. In spite of the fact that these expressions are based on the weakly guiding fibre approximation, i.e. small difference of refractive index between the core and the cladding  $(n_{\text{core}}^2 - n_{\text{cladding}}^2)/(2 \times n_{\text{core}}^2) \ll 1$ , we propose to apply them to our water-jet waveguide.

Looking at Figures 3 and 4 we can see that the grain size of the intensity modulation is quite homogeneous over the jet cross-section for a set of given coupling conditions. The origin of the modulation is the superposition of many, statistically phase shifted, guided fibre modes. In the middle of the water jet all excited modes have contributions and the resulting grain size of the interference pattern is difficult to describe. On the border of the jet however, only the highest order modes make substantial contributions to the intensity distribution. As a consequence, we can say that the (constant) size of the grains is given by the period of the intensity modulation of the highest order modes close to the border of the waveguide core.

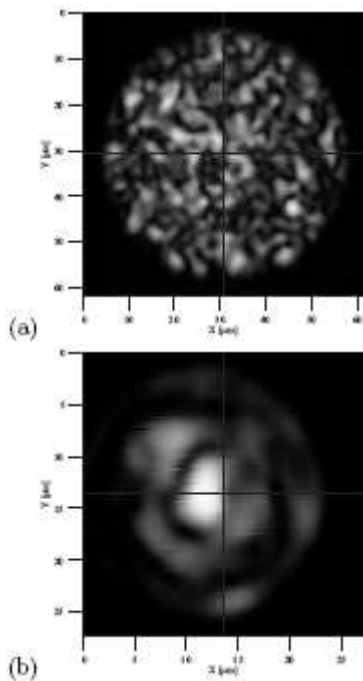


**Fig. 4** Influence of jet diameter on the intensity distribution. (NA=0.16, minimum off-axis, jet distance 35 mm); (a) 65  $\mu\text{m}$  nozzle, jet velocity 187m/s; (b) 29  $\mu\text{m}$  nozzle, jet velocity 281 m/s

In order to determine the modulation period, we need to calculate the normalized frequency (or V-factor) of the waveguide of radius  $\alpha$  under the given coupling conditions, i.e. the used numerical aperture, NA, and the wavelength of the guided light,  $\lambda_0$ .

$$V = \frac{\pi 2aNA}{\lambda_0} \quad (1)$$

with  $2\alpha$  as the waveguide diameter and  $\lambda_0 = 632 \text{ nm}$  for He-Ne laser.

Restricting ourselves, as in the case of weakly guiding fibres, to the linearly polarized modes  $LP_{lm}$ , the maximum mode numbers  $l$  and  $m$  are given by:

$$l = \frac{2V}{\pi + 1} \text{ and } m = \frac{V}{\pi} \quad (2)$$

The total number of modes in the waveguide are given approximately by:

$$N = \frac{4V^2}{\pi^2 + 2} \quad (3)$$

and the corresponding maximum theoretical grain size  $\delta_l$  and  $\delta_m$  are defined as:

$$\delta_l = \frac{2a\pi}{2l} \text{ and } \delta_m = \frac{2a}{2m} \quad (4)$$

The experimentally determined characteristic modulation wavelength  $\lambda_N$  can be compared to the values. Table 2 shows the results of this comparison for the 112- $\mu\text{m}$  nozzle, a He-Ne laser at 632 nm and the different coupling NA's. The fill factor of the fibre, defined as the ratio between the number of excited modes and the maximum possible number of modes, is also indicated in the table for all coupling conditions.

The results show that the experimental grain size values are larger than the calculated ones. Nevertheless, the values are comparable and it is confirmed that the higher the NA the lower the characteristic modulation wavelength.

**Table 2** Characteristic modulation wavelength of modal noise for various NA, nozzle diameter 112  $\mu\text{m}$ , and laser wavelength  $\lambda_0 = 632 \text{ nm}$ .

NA	Grain size	$\delta_l$	$\delta_r$	Fill factor $N/N_{\text{max}}$
0.06	$\lambda_N \approx 6 \mu\text{m}$	8.3 $\mu\text{m}$	5.6 $\mu\text{m}$	0.46 %
0.16	$\lambda_N \approx 4 \mu\text{m}$	3.1 $\mu\text{m}$	2 $\mu\text{m}$	3.3 %
0.29	$\lambda_N \approx 2.2 \mu\text{m}$	1.8 $\mu\text{m}$	1.2 $\mu\text{m}$	10 %

### 4. Experimental verification

A Q-switched Nd:YAG laser is used in this study ( $M^2 = 1.2$ ) emits at 1064 nm wavelength. The laser pulse duration is approximately 50 ns with a peak power of 50 kW. The focussed laser spot diameter is approximately 30  $\mu\text{m}$ . The maximum average output power is 17 W. To reveal the energy distribution in the jet waveguide, ablation of a thin steel plate is studied with different numbers of laser pulses.

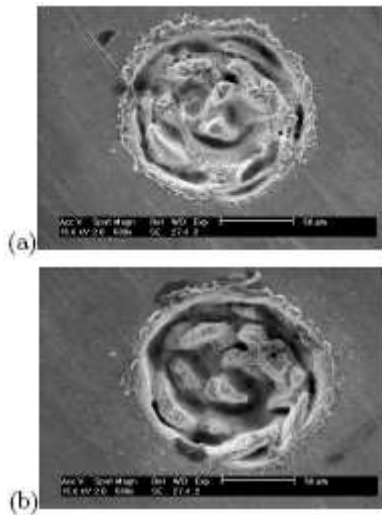


**Fig. 5** Ablation of a 400  $\mu\text{m}$  steel plate; 150  $\mu\text{m}$  nozzle,  $\text{NA}=0.03$ , jet velocity 94 m/s, average power 7 W at 1.5 kHz; (a) 10 pulses; (b) 50 pulses

As shown in the SEM images (Fig. 5), despite ablation structures being rather complex, we note that they are almost identically reproducible and do not depend on the number of laser pulses. The structures present strong similarities with the intensity distributions observed in the water jet waveguide.

Comparing the theoretical grain sizes  $\delta_1$  and  $\delta_m$  values (24  $\mu\text{m}$  and 21  $\mu\text{m}$ , respectively) to the size of the structures being in the range of 10 to 20 microns we once more confirm good agreement between the applied model and the experimental observations.

## 5. Recent micromachining examples with the LMJ

### 5.1 Percussion drilling of blind holes in silicon wafers

Fig. 6 shows the consistency of the drilling results on a 600  $\mu\text{m}$  thick bare silicon wafer using a third harmonic 355 nm UV laser.

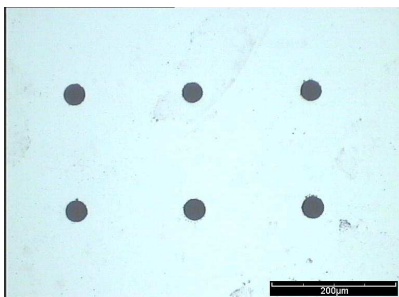


**Fig. 6:** A hole matrix, top view, 30  $\mu\text{m}$  nozzle, 90 kHz, 9 W, 20 holes/s

The average measured hole diameter is 35  $\mu\text{m}$ . The hole circularity is about 0.9. With no post cleaning steps, the holes are clean and free of debris, burrs, cracks and thermal damage. The hole diameter at the bottom is about 15  $\mu\text{m}$ . The depth of the holes is approximately 50  $\mu\text{m}$ .

Results of hole drilling on a 300  $\mu\text{m}$  device wafer are illustrated in Fig. 7. A second harmonic 532 nm laser was used for this application.

The hole diameter is about 15% bigger than the nozzle size. This widening is due to the ejected material. The drilling rate is 25 holes/second. The drilling depth in all case is about 140-150 $\mu\text{m}$ . The holes have a slight taper and the bottom of the holes have a rounded conic shape.

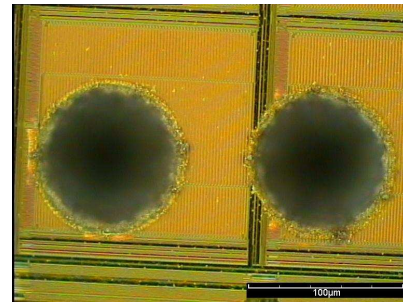


**Fig. 7:** Microscopic image of two holes drilled with a 80  $\mu\text{m}$  nozzle, 34 W, 40kHz.

Very small holes were also generated on the metallic contact pads of a 700  $\mu\text{m}$  thick device wafer shown in Fig. 8. A 1070  $\mu\text{m}$  fiber laser was selected for this experiment, producing 70  $\mu\text{m}$  deep and 30  $\mu\text{m}$  diameter holes.

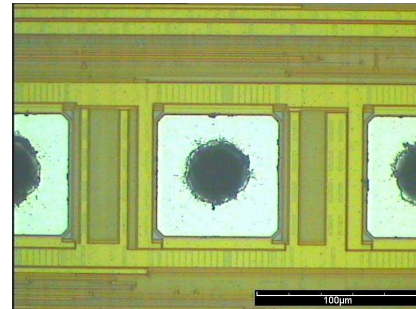


**Fig. 8:** Holes drilled in metallic contact pads, 25  $\mu\text{m}$  nozzle, 26W, 50 kHz, 30 holes/s

### 5.2 Grooving of sapphire wafers

Grooving of a 350  $\mu\text{m}$  thick sapphire wafer to a depth of about 110  $\mu\text{m}$  was achieved with superior edge quality and regular depth as shown below in Fig. 9. No chipping or contamination occurred. The grooving width is approximately 55  $\mu\text{m}$ .

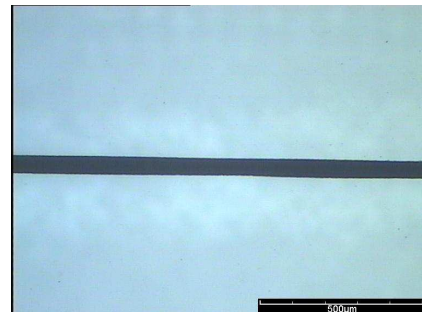


**Fig. 9:** Microscopic image of a groove, 355 nm UV laser, 9.5 W, 20 kHz, 50  $\mu\text{m}$  nozzle, overall speed 10 mm/s

## 6. Summary

The numerical aperture of the coupling of the laser source into the water jet waveguide is the predominant parameter influencing the grain size of modal noise in intensity distributions. The number of modes i.e. the reduction of the size of the intensity grains is clearly increased with increasing NA so that the modes are well distributed over the jet cross section. For centred coupling, the intensity at the jet centre is higher than those at the jet periphery. A better homogeneity of the modes over the entire water jet section is obtainable by de-centring the coupling. The predicted intensity grain sizes are in good agreement with the experimental ones. Finally, the modal noise in the water jet waveguide partly explains the ablation process of the Laser-Microjet technology.

Lastly, the LMJ is also suitable for percussion hole drilling with no problems of water jet disturbance. Excellent results of sapphire grooving with a UV LMJ have also been demonstrated. Conclusion: the LMJ is an excellent tool for many micromachining applications.

## References

- [1] Richerzhagen B. (2001) Chip singulation process with a water-jet guided laser, *Solid State Technology* 44(4), S25–S28.
- [2] Snyder A.W. & Love J.D. (1983) *Optical Waveguide Theory*, Chapman and Hall, New York.
- [3] Snyder A.W. (1972) Coupled mode theory for optical fibers, *J. Opt. Soc. Am.* 62(11), 1267.
- [4] Epworth R.E. (1978) The phenomenon of modal noise in analogue and digital fiber systems, in *Proc. 4th European Conf. Optic. Commun.*, Genoa, Italy, 492–501 Sept.
- [5] Wang Qi, Ning Y.N., Grattan K.T.V. & Palmer A.W. (1995) Effect of Multimode Fiber Core Diameter on Modal Noise Suppression in White-Light Interferometry, *Opt. Commun.* 118(5-6), 473–478.
- [6] Kuhn A., Blewett I.J., Hand D.P. & Jones J.D.C. (2000) Beam quality after propagation of Nd:YAG laser light through large core optical fibers, *Appl. Opt.* 39(36), 6754–6760.
- [7] Sterling A.M. & Sleicher C. A. (1975) The instability of capillary jets, *J. Fluid Mech.* 68(3), 477–495.
- [8] Couty Ph., Vago N., Spiegel A., Ugurtas B.I. & Hoffmann P. (2003) Laser induced break-up of water-jet waveguide, *In press Exp. Fluids*.
- [9] Spiegel A., Vago N. & Wagner F.R. (2004) High efficiency Raman scattering in micro water jets, *In press Opt. Eng.* 43(2).
- [10] Vennard J.K. & Street R.L. (1976) *Elementary Fluid Mechanics*, John Wiley & Sons, New York, 157-158; 557-563.
- [11] Saleh B.E.A. & Teich M.C. (1991) *Fundamentals of Photonics*, John Wiley & Sons, 272–287.